CALIBRATING BASIN-SCALE GROUNDWATER MODELS TO REMOTELY SENSED ESTIMATES OF GROUNDWATER EVAPOTRANSPIRATION

Rosemary W.H. Carroll, Desert Research Institute
Greg M. Pohll, Desert Research Institute
Charles G. Morton, Desert Research Institute
Justin L. Huntington, Desert Research Institute

Summary

Increased population pressures, climate change and limited water resources in the arid and semi-arid southwestern United States require managers to properly account for basin-scale water balances, in which phreatophytic and riparian consumption of groundwater is an important component. Remotely sensed vegetation indices correspond to canopy vigor and cover through the ratio between red and near infrared in the electromagnetic spectrum, and have been successfully used to estimate groundwater evapotranspiration (ET_g) over large spatial and temporal scales. However, these data do not provide information on depth to groundwater (*dtgw*) necessary for groundwater models to calculate ET_g. Assuming an exponential decline in ET_g with *dtgw*, an iterative approach is provided that calibrates MODFLOW to ET_g derived from Landsat estimates of the Enhanced Vegetation Index (EVI). The approach is applied to different functional groups in Mason Valley, Nevada over an eleven year time span, and accounts for atmospheric water demand. An uncertainty analysis is done to estimate the resulting mean and 90% confidence intervals in ET_g to *dtgw* relationships, while a first-order second moment analysis shows these relationships are almost exclusively sensitive to estimated land surface ET_g despite relatively large uncertainty in extinction depths and hydraulic conductivity. Results are verified with site specific water level data. Combining vegetation mapping, remotely sensed estimates of ET_g and basin-scale groundwater models will aid researchers in deciphering eco-hydrologic responses to changing water conditions and can provide regional managers the necessary tools to make informed decisions on water resource allocations into the future.

TABLE OF CONTENTS

LIST OF FIGURES

LIST OF TABLES

INTRODUCTION

Water shortages caused by population growth, climate change and limited water supply in the semi-arid and arid southwest of the United States have water managers searching for additional sustainable sources of water from many of the regions undeveloped basins. Groundwater discharge from these basins is often dominated by phreatophytic groundwater evapotranspiration (ET_g). Despite relatively low ET_g rates for phreatophyte communities, large acreage of these communities across valley floors translates into significant volumes of water lost at the regional scale (Nichols, 1994; 2000). Properly quantifying ET_g is paramount for water managers to accurately calculate water budgets in these closed basins. Historic estimates of evapotranspiration (*ET*) (e.g. Malmberg and Eakin, 1962; Walker and Eakin, 1963; Malmeberg, 1967 Rush, 1968) were susceptible to inaccurate estimates of acreage and possible error in estimated annual *ET* rates. Relatively contemporary efforts in the Death Valley region (Laczniak et al., 2001), Ash Meadows, Nevada (Laczniak et al., 1999) and elsewhere in Nevada (e.g. Maurer et al. 2005; Moreo et al., 2007; Allander et al., 2009; Huntington et al., 2011) have improved upon estimated rates using micrometeorologic, energy balance and complementary approaches; however, these approaches are limited to point measurements. Scaling point measurements across the landscape, however, has been successfully done by correlating remotely sensed vegetation indices to phreatophytic micrometerologic data (Nagler et al., 2005; Groeneveld et al., 2007; Allander et al., 2009; Beamer et al, in press).

Depth to groundwater (*dtgw*) is often cited as the principal factor controlling ET_g in phreatophyte communities (Devitt et al., 2002; Nichols, 1994; 2000), with the basic assumption that higher ET_g occurs at shallower water table depths. Most closed or partially closed basins in the Great Basin have a central playa with a shallow water table. Saltgrass (*Distichil spicata* var. stricta) tends to grow along the margins of these playas with *dtgw* generally less than 2.5 m (Nichols, 1994) but found to grow in areas with *dtgw* = 3.6 m (Blaney et al., 1933). Greasewood (*Sarcobatus vermiculates*) also grows along the margins of these playas, but can also proliferate in basins with no playa. Depth to groundwater in greasewood communities ranges from 1.5 m to 11 m and potentially reaches 18 m (Robinson, 1958). Along with riparian vegetation, greasewood is the principal phreatophyte in the Great Basin, with an extensive range away from the playa margins, and consuming the most groundwater (Nichols, 1994).

Simple functions, or piecewise functions, of ETg to dtgw are often used to estimate ETg and applied at the landscape scale using maps of water table depth calculated with groundwater models. Unfortunately, numeric modeling approaches tend to ignore other factors that control ETg, such as plant canopy cover, leaf area, community composition, and soil water holding capacity. While remotely sensed vegetation indices correspond to canopy vigor and cover primarily through the ratio between red and near infrared wavelengths of the electromagnetic spectrum, these data do not provide information on dtgw necessary for

groundwater models. The objective of this study is to provide a methodology to bridge this information gap between remotely sensed vegetation indices and basin-scale groundwater models. The approach is iterative because groundwater models require the ETg to dtgw function known a priori. Calibrated ETg to dtgw functions are then evaluated at the 90% confidence interval (CI) for different phreatophytic and riparian functional groups.

Relevance to the Walker Lake Restoration Program

Surface and groundwater interactions are an important aspect of the decision support tool (DST) and have broad implications to water rights management. A better understanding of how well the current groundwater model predicts these interactions will provide insight on potential areas for improvements. This research identifies the importance of calibrating groundwater models to water levels, stream flow, and phreatophyte ET. This work provides better estimates of phreatophyte ET and will improve our understanding of the impacts of water rights transfers on the complex hydrologic system in Mason Valley.

Site Description

Figure 1 shows the demonstration site, Mason Valley, located in the Walker Basin. The Walker Basin straddles the California-Nevada state line, occupying portions of Mono County in California, and Lyon, Mineral, Douglas, and Churchill counties in Nevada. The East and West forks of the Walker River originate in California in the eastern Sierra Nevada and flow north-northeast before converging in Mason Valley just south of Yerington, Nevada. Upon exiting Mason Valley the river turns southward before terminating in Walker Lake. Mason Valley is the largest irrigated agricultural area within the Walker River Basin, and includes irrigated areas along the West Walker, East Walker and main Walker rivers. All crop irrigation and groundwater development in Mason Valley occur on the alluvium, which consists of unconsolidated gravel, sand, silt and clay (Huxel and Harris, 1969; Hess and Johnson, 1997). The total area of Mason Valley alluvium is 595 km^2 (147,030 acres). Groundwater pumping supplements existing surface water rights. Figure 1 inset shows irrigation wells in production from 1996 to 2006. Wells are primarily screened in the upper 130 m of alluvium, below which lies older alluvium and fan deposits with transmissivities assumed to be significantly lower than that of the surficial deposits (Huxel and Harris, 1969).

Climate in the basin is characterized as arid with cold/wet winters and hot/dry summers. Temperatures vary substantially at the seasonal and diurnal scale, which is common among desert environments. The Wabuska meteorological station (5Se COOP, 268822) is located at an elevation of 1310 m and is situated where the river exits Mason Valley. The meteorological station indicates that, on average, maximum monthly temperatures occur during August at 34.2 °C, while the minimum monthly average temperature occurs in January at -8.8°C. Average annual precipitation in the basin is equal to 0.118 m/yr.

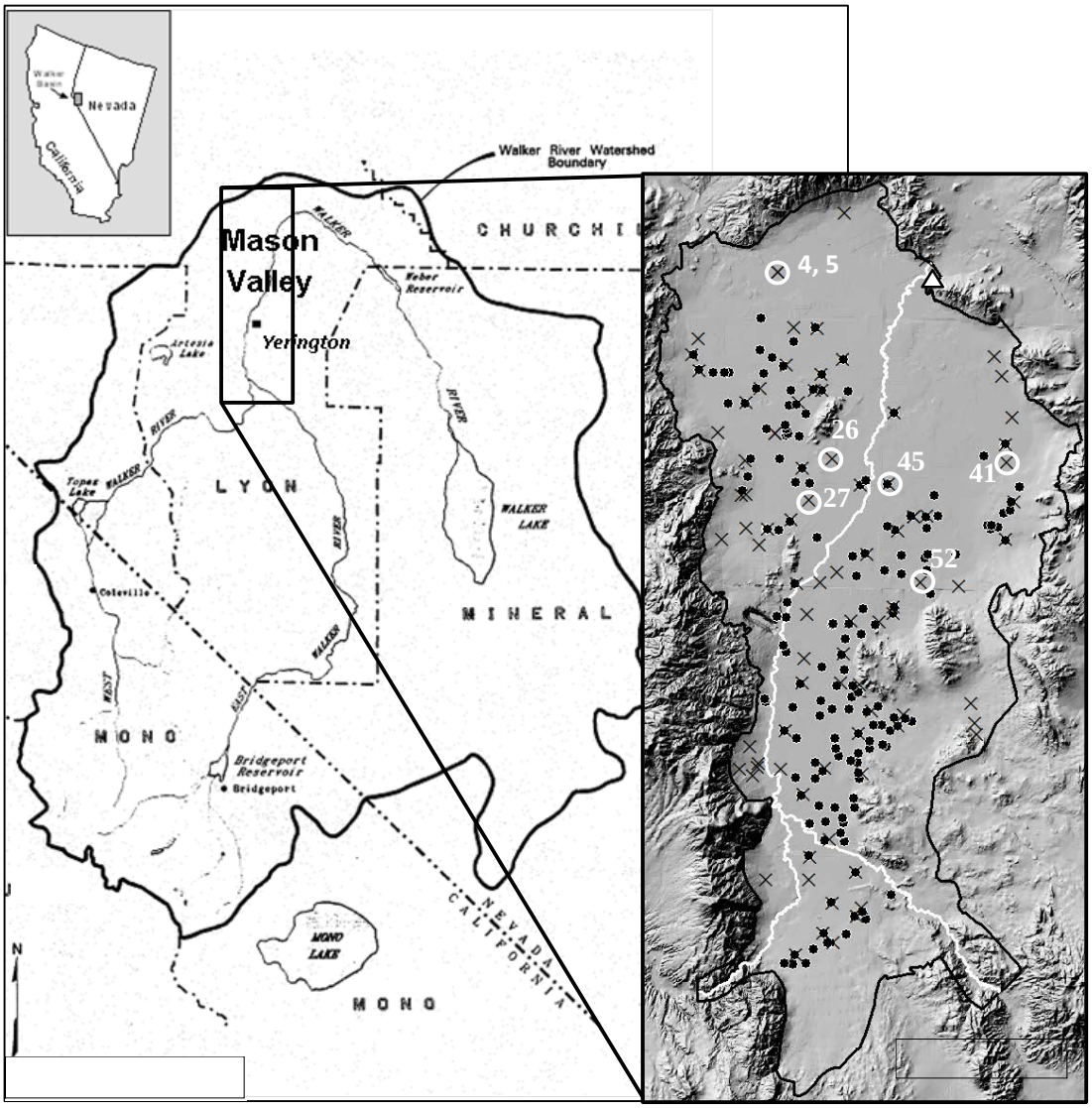

Figure 1. Walker River Basin, with Mason Valley marked and expanded to show pumping wells (black dots), wells with observed water level data (black crosses) and wells with observed water level data where groundwater evapotranspiration (ETg) is modeled (white circles with well ID). The Walker River is shown as a white line. The Wabuska meteorological station (5Se COOP, 268822) is located at the river's exit from the northern basin (solid white triangle). The small inset shows the location of the Walker River Basin with respect to California and Nevada in the western United States.

Vegetation in the valley is mapped in Figure 2. Non-agricultural areas are those that contain wetlands/open water, phreatophyte, or riparian vegetation. Phreatophytic zones are separated into two functional groups based on dominant species: saltgrass and greasewood (Huxel and Harris, 1969). Phreatophytes are relatively extensive in the northern portion of Mason Valley near the Nevada Division of Wildlife wetlands, as well as the marshy zone near the Adrian Gap at the northwestern quadrant of the basin. Riparian zones are based on the combined spatial extent of riparian areas mapped for six different years (1986, 1992, 1995, 1998, 2000, and 2002) using satellite imagery collected by the Thematic Mapper (TM)

sensor on the Landsat 5 satellite (Minor et al., 2006). Riparian zones are interspersed between wetland regions and along the river corridor.

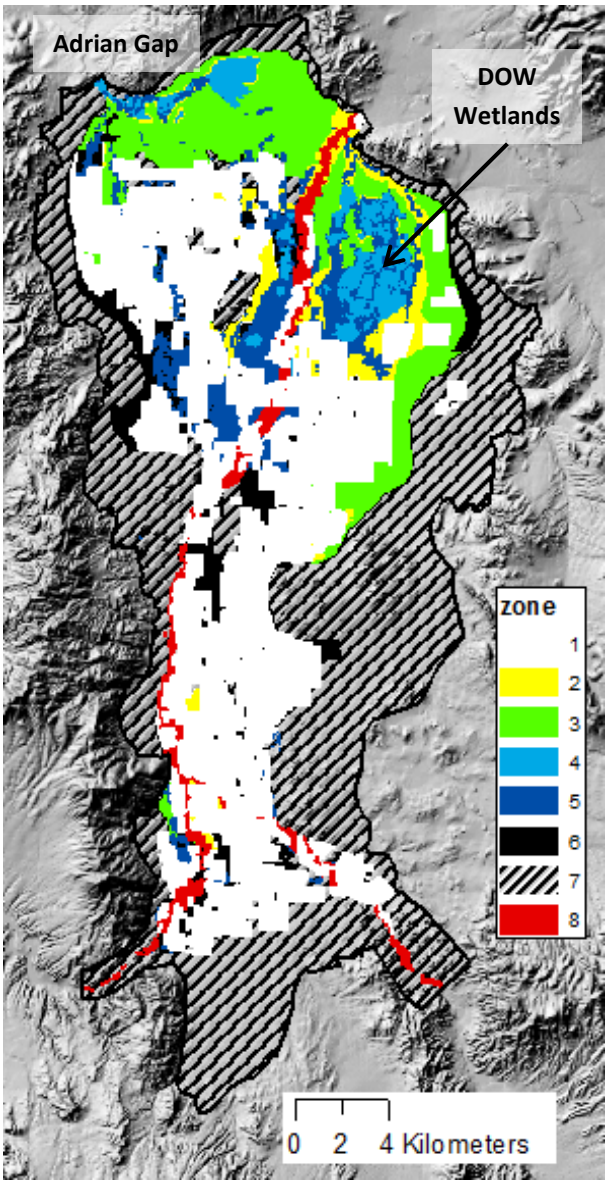

Figure 2. Functional vegetation groups assigned by dominant species: zone 1 = agriculture; zone 2 = saltgrass; zone 3 = greasewood; zone 4 = wetland and open water along with mixed phreatophyte; zone 5 = wetland riparian; zone 6 = non-phreatophyte; zone 7 = valley fill; and zone 8 = river riparian.

Groundwater Model

Carroll et al. (2010) developed a groundwater model (GWM) of the Mason valley basin using MODFLOW-2000 (Harbaugh et al., 2000) with a 100 m grid size and monthly stress periods. Readers are referred to Carroll et al. (2010) for a detailed description of model development and its original calibration. Agricultural *ET* is satisfied with irrigated waters and stored soil moisture derived from precipitation and does not obtain any water needs from the groundwater. Non-agricultural lands, however, are assumed to use stored soil moisture and groundwater to satisfy consumptive needs. The exceptions include the non-phreatophyte and valley fill functional groups (zone 6 and 7, Figure 2) which do not access groundwater but are assumed to survive only on soil moisture.

Carroll et al. (2010) calculated ET_g using MODFLOW's evapotraspiration (EVT) package in which one assumes a linear decline in ET_g with increased *dtgw* (Figure 3). The EVT package requires three input parameters: PET_g, the maximum, or potential groundwater evapotranspiration (L/T); *dx*, extinction depth at which ET_g is zero (L); and *ds*, the elevation (L) for which ET_g is at a maximum. Carroll et al. (2010) defines monthly PET_g rates with data collected by Maurer and Berger (2005; 2006) and adjusted for long-term average monthly precipitation in Yerington (WRCC, 2007). Annualized PET_g rates were equal to 0.44 m/yr for phreatophytes, 0.94 m/yr for riparian vegetation, and 1.21 m/yr for perennial wetlands. The ET_g surface (*ds*) was defined by the mean land surface elevation for each model cell, while an extinction depth equal to 10.0 m was assigned to all phreatophytes, and 1.0 m to perennial wetlands and riparian vegetation. Carroll et al. (2010) preformed no calibration with respect to ET_g in the GWM.

With no calibration, modeled annual water balances indicate that ET_g accounts for 5-16% of the losses from the system, with an average loss of 34 million m^3/yr (27,500 acre-ft per year, AFY). In general, ET_g is the third largest water loss from the basin, behind river outflows and crop *ET*. However, during drought years ET_g surpasses river outflows and constitutes the second largest loss from the system.

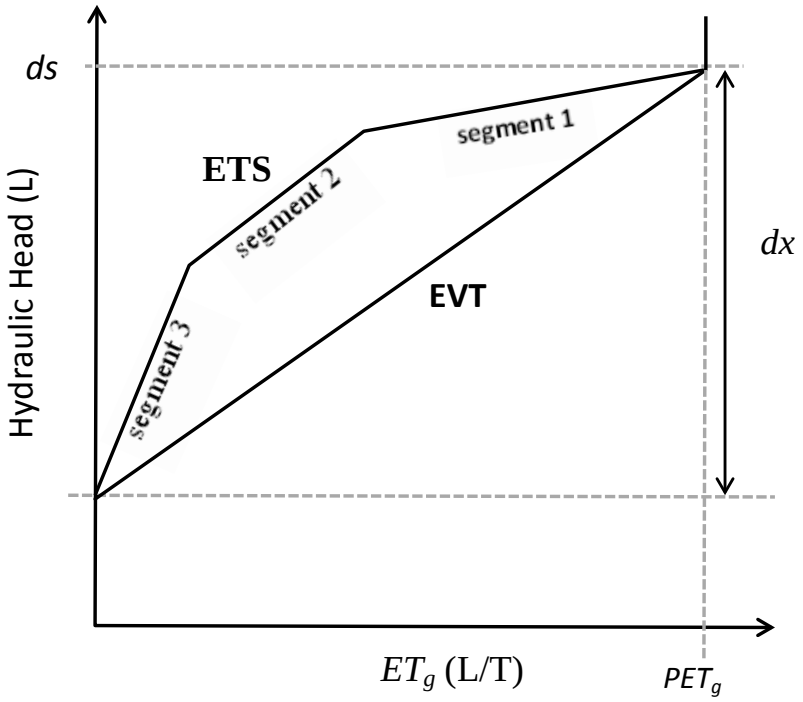

Figure 3. MODFLOW functional definition for ET_g as a function of hydraulic head in the EVT package (linear) and the ETS package (segments). ET_g = groundwater evapotranspiration, PET_g = maximum, or potential ET_g, ds = ET_g surface elevation for which ET_g is at a maximum, dx = extinction depth. If ds = land surface, then ds minus hydraulic head equals depth to groundwater (*dtgw*).

Methodology

Landsat Derived Groundwater Evapotranspiration

The Enhanced Vegetation Index (EVI) is selected over the Modified Soil Adjusted Vegetation Index (MSAVI) and the Normalized Difference Vegetation Index (NDVI) based on work by Beamer et al. (in press) who found EVI the best predictor of phreatophyte shrub ET_g in Nevada. EVI also improves vegetation monitoring by decoupling the canopy background signal and reducing atmospheric influences (Huete et al., 2002). The vegetation index is derived from Landsat 5 Thematic Mapper (TM) and Landsat 7 Enhanced Thematic Mapper Plus (ETM+) imagery. The TM and ETM+ radiometers collect in three visible, one near-infrared, two shortwave infrared and one thermal infrared bands. The visible and shortwave bands have a 30 m pixel size while the thermal band pixel size is 60 m for TM and 120 m for ETM+. The raw imagery was radiometrically and atmospherically corrected to at-surface reflectance using the Landsat Ecosystem Disturbance Adaptive Processing System (LEDAPS) (Masek et al. 2006).

EVI is calculated as,

$$EVI = \mathrm{G} \times (\rho_{NIR} - \rho_{Red})/(\rho_{NIR} + \mathrm{C}_1 \times \rho_{Red} + \mathrm{C}_2 \times \rho_{Blue} + \lambda) \quad (1)$$

where ρ is the at-surface reflectance, *NIR* is near infrared waveband from 0.76 to 0.90 μm, *Red* is waveband from 0.63 to 0.69 μm, *Blue* is waveband from 0.45 to 0.52 μm. λ is the canopy background adjustment that addresses nonlinear, differential *NIR* and *red* radiant transfer through a canopy, and C_1, C_2 are the coefficients of the aerosol resistance term, which uses the blue band to correct for aerosol influences in the red band. The coefficients adopted in the EVI algorithm are, λ=1, C_1=6, C_2 = 7.5, and *G* (gain factor) = 2.6 (Nagler et al., 2005).

Previous studies suggest that the time period from June to August is the most representative period to characterize peak health and vigor of phreatophyte vegetation in the Great Basin (Allander et al., 2009; Groeneveld et al., 2007; Smith et al., 2007). Mid-summer Landsat TM and ETM+ scenes (Path 42/ Row 33) were selected by the following criteria: (1) the scenes are completely clear of cloud/smoke within the delineated phreatophyte boundary, (2) there has been no major precipitation event in the two weeks leading up to scene acquisition, and (3) the vegetation signal from the phreatophyte areas is easily distinguished (i.e. greener, high EVI) from the surrounding non-phreatophyte areas, which indicates plants are utilizing shallow groundwater stores. From all viable images satisfying these three criteria, a single representative scene is chosen that is coincident with the highest daily reference evapotranspiration (ET_o), as calculated with the ASCE Standard Penman-Montieth

equation for a grass reference surface (ASCE-EWRI, 2005; Huntington and Allen, 2010; Allen, 2011).

Groeneveld et al. (2007) and Beamer et al. (in press) assume a normalized ET^* as,

$$ET^* = \frac{(ET - PPT)}{(ET_o - PPT)} \quad (2)$$

where *ET* is the total annual evapotranspiration demand for phreatophytes and *PPT* is annual precipitation. ET^* is also computed from EVI as,

$$ET^* = \beta_0 + \beta_1 EVI + \beta_2 EVI^2, \quad (3)$$

per 30 m pixel then averaged up to the 100 m model grid. The scaling up process occurs with ET*, not EVI, given the non-linear relationship of equation 3. Coefficients β_0, β_1, β_2 equal -0.196, 2.904, and -1.592 (Beamer et al., in press). Rearranging equation 2,

$$ET = (ET_o - PPT)ET^* + PPT, \quad (4)$$

and subtracting the annual *PPT* from total *ET,* yields the groundwater component, or ET_g,

$$ET_g = (ET_o - PPT)ET^*. \quad (5)$$

Groundwater Model ET_g

Research suggests a non-linear response of ET_g with respect to *dtgw* (e.g. Nichols, 1994; Cooper et al., 2006; Shah et al., 2007; Groeneveld, 2008). MODFLOW's segmented evapotranspiration package (ETS) (Banta, 2000) allows for a more complex functional response in ET_g with declining water levels compared to the EVT package (Figure 3). The ETS requires the same three input parameters needed for the EVT package, but in addition one must also designate the number of segments as well as the coordinates of each segment's vertices as fractions of PET_g and *dx*. Similar to Carroll et al. (2010), the ET_g surface (*ds*) is assumed land surface. To account for annual variation in atmospheric water demand, monthly PET_g is tracked by subtracting monthly *PPT* at the Wabuska COOP station from the monthly sum of ET_o.

It is assumed that the ET_g functional form is exponential with depth (e.g. Nichols, 1994; Shah et al., 2007) such that,

$$\psi = \alpha e^{-\beta * dtgw}, \quad (6)$$

where $\psi = ET_g/PET_g$. The coefficient α scales grass reference PET_g (i.e. $PET_g = ET_o$-*PPT*) to the maximum ET_g at land surface for the functional group considered. While PET_g changes in time, the ratio ψ is assumed temporally constant at a given *dtgw*. β controls the extinction depth (*dx*) such that,

$$dx = -\frac{\ln(\phi)}{\beta}, \quad (7)$$

where ϕ is the assumed fraction of PET_g at which ET_g is negligible. For this study ϕ is assumed to equal 0.5%.

Observed ET_g to *dtgw* Relationships

Seven wells with observed water level data (n = 34) are coincident with GWM cells for which ET_g is modeled (refer to Figure 1). Water level data are matched with EVI estimated ET_g for the modeled cell that contains the observation well. ET_g is normalized by the annual grass reference PET_g for comparison with GLUE derived means and confidence intervals (CI).

Uncertainty Analysis

The generalized likelihood uncertainty estimate (GLUE) methodology (Beven and Blinley, 1992) is based on a normalized objective function from Blasone et al. (2008),

$$F_j(\vec{\theta}_j) = \sum_{i=1}^{I} \frac{Q_i(\vec{\theta}_j)}{(Q_i)_{min}}, \quad (8)$$

where $F_j(\vec{\theta}_j)$ is the aggregate objective function for the j^{th} randomly selected parameter vector $\vec{\theta}$, $Q_i(\vec{\theta}_j)$ is the root mean squared error (*rmse*) for the i^{th} criteria given the parameter set $\vec{\theta}_j$, and $(Q_i)_{\min}$ is the minimum computed *rmse* for the i^{th} criteria given all realizations. The resultant likelihood function for $\vec{\theta}_j$, given *J* total realizations, is compared to the vector of observed data $\vec{Y}$ with,

$$L_j(\vec{Y}|\vec{\theta}_j) = c\left(\frac{1}{F_j(\vec{\theta}_j)}\right)^N. \quad (9)$$

The constant *c* normalizes the likelihood function such that $\sum_{j=1}^{J} L_j(\vec{Y}|\vec{\theta}_j) = 1$. Therefore *c* is defined as,

$$c = \frac{1}{\sum_{j=1}^{J} L_j(\vec{Y}|\vec{\theta}_j)}. \quad (10)$$

Within equation 9, *N* is a subjective shape factor often used in a GLUE likelihood function to tighten or widen estimated CIs. As *N* approaches 0, the likelihood function yields equal likelihoods (or weights) for all realizations (1/*J*) and GLUE is analogous to traditional Monte Carlo analysis. As *N* approaches infinity, the best fitting realization obtains a likelihood value of 1.0, and all other realizations receive a weight of 0, and the problem is equivalent to an inverse solution. Similar to Franks et al. (1999) *N* is adjusted such that the 90% confidence interval in modeled ET_g captures 90% of the annual EVI derived ET_g data for all functional groups. The 90% CI is computed by summing the ranked likelihood values in equation 9 to 0.05 and 0.95 for the lower and upper bound, respectively.

The resultant GLUE estimated posterior distribution means (μ_l) and standard deviations (σ_l), for the l^{th} input parameter given J realizations, are calculated as the sums,

$$\mu_l = \sum_{j=1}^{J} L_j\left(\vec{Y}\middle|\vec{\theta}_j\right)\vec{\theta}_{j,l}. \tag{11}$$

$$\sigma_l = \sum_{j=1}^{J} L_j\left(\vec{Y}\middle|\vec{\theta}_j\right)\left(\vec{\theta}_{j,l} - \mu_l\right)^2. \tag{12}$$

Relative uncertainty (U) is computed for each input parameter (θ_l) using the first-order second-moment (FOSM) approach,

$$U_{i,l}(\vec{Y}|\theta_l) = \sigma_l^2\left(\frac{dQ_{i,l}}{d\theta_l}\right)^2 \tag{13}$$

Input parameters are evaluated independently by adjusting the GLUE derived means of *HK*, α and *dx* by ±1%. Linearity is required for first-order analysis. The small percentage adjustment in parameter values is an attempt to maintain linearity in model response by limiting the range in which it's asked to perform. Relative uncertainty ($U^*_{i,j}$) is normalized such that the sum of all relative uncertainty for a specific criteria (i) equals 1.0. The *rmse* ($Q_{i,l}$) is defined at the global level and for each functional group.

Given the potentially complex interaction between hydraulic conductivity (*HK)*, *dtgw* and ET_g, two modeling scenarios are performed to determine the influence of *HK* on predicting the ET_g to *dtgw* curves. These scenarios include: (1) allowing coincident uncertainty in *HK*, α and β, and calculating an $F_j\left(\vec{\theta}_j\right)$based on observed water level data (n = 816) and annual EVI derived ET_g for each functional group (n = 55), and (2) maintaining the calibrated *HK* while allowing uncertainty in α and β, and using only EVI derived ET_g in the objective function. One thousand realizations are run assuming the calibrated values of *HK*, α and *dx* equal the input parameter prior distribution means.

Results and Discussion

Model Calibration

EVI image dates are provided in Table 1 along with annual sums of *PPT* and ET_o. All image dates fall within the summer months of June to August and meet the selection criteria discussed in the methodology section. Late summer image dates are used during years containing above average summer precipitation, while all other years are assigned image dates pertaining to that date with the highest daily ET_o.

Table 1. Selected EVI image dates along with water year totals of precipitation (PPT), grass reference evapotranspiration (ETo) and resultant potential groundwater evapotranspiration (PETg)

Year	Image Date	PPT m/yr	ET_o m/yr	PET_g m/yr
1996	8/11	0.158	1.287	1.129
1997	6/25	0.136	1.258	1.122
1998	8/15	0.223	1.227	1.004
1999	7/17	0.052	1.216	1.164
2000	6/11	0.078	1.272	1.194
2001	6/12	0.062	1.301	1.239
2002	6/7	0.076	1.356	1.279
2003	6/10	0.081	1.352	1.271
2004	7/15	0.082	1.388	1.306
2005	8/18	0.155	1.269	1.114
2006	8/21	0.141	1.371	1.230

With no model calibration of ET_g (Carroll et al., 2010), the GWM regression of ET_g has a slope of -0.2 and only describes 2% of the observed variation (Figure 4). Poor model prediction is further exemplified in Figure 5, which shows that the un-calibrated GWM over predicts total ET_g in saltgrass, greasewood and river riparian zones, by 19 Mm^3, 75 Mm^3 and 28 Mm^3, respectively, while under predicting wetland and wetland riparian communities by 72 Mm^3 and 98 Mm^3.

For comparison, Figures 4 and 5 show results given GWM calibration of ET_g. Calibration is accomplished by maintaining *HK* from Carroll et al. (2010) and adjusting α and *dx* in equation 6 and 7 such that the regression in Figure 4 produces a slope of 1.0 and intercept equal to 0.0. The calibrated GWM explains 87% the expected variability in ET_g and model performance is significantly improved for all functional groups.

Despite model improvement, the model does not replicate annual variability seen in each functional group. This is especially true for the saltgass and greasewood communities. GWM predicted ET_g is driven by PET_g and *dtgw*, neither which show large variability from year to year, and predicted ET_g is fairly constant in time. In contrast, remotely sensed EVI produces approximately 60% increases in ET_g during 1998, 2005 and 2006 compared to other years. Why the large increase in EVI derived ET_g during these specific years? Each of these years experienced above average precipitation with 1998 receiving nearly twice the long term average at 0.223 m/yr. However, annual *PPT* is removed from the EVI derived ET_g (eq. 5)

as well as from the ET_o time series to define PET_g in the GWM. For any given ET_o, a larger *PPT* should lower both the EVI and GMW estimated ET_g. The discrepancy may not be related to the quantity of *PPT*, but to the timing of *PPT*. For those years in question, the fraction of annual *PPT* falling in May and June is significantly greater than the long term average for the basin. As an example, May and June *PPT* in 1998, is more than four times higher than the long term average (Figure 6). The late spring-summer precipitation causes a "greening" of phreatophyte shrubs not correlated to groundwater uptake.

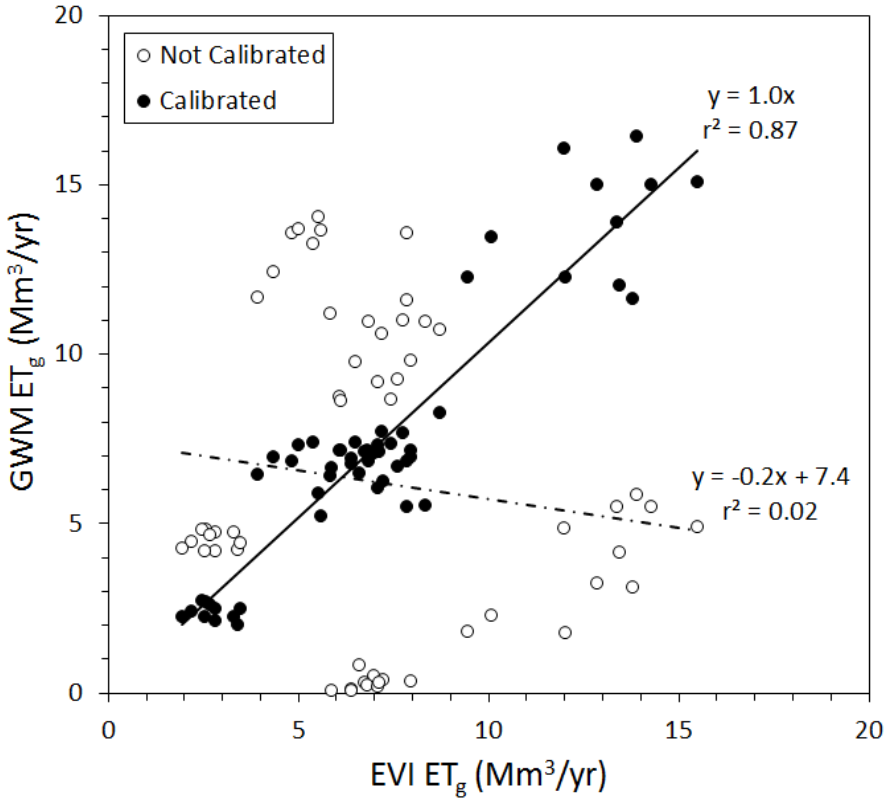

Figure 4. A comparison of groundwater model (GWM) and remotely sensed (EVI) estimates of annual ET_g in millions of cubic meters per year (Mm^3/yr) for years 1996 to 2006 given each vegetation zone (n=55). The regression for calibrated results is shown as a solid black line. The regression for original, uncalibrated, GWM (Carroll et al., 2010) is given as a dashed black line.

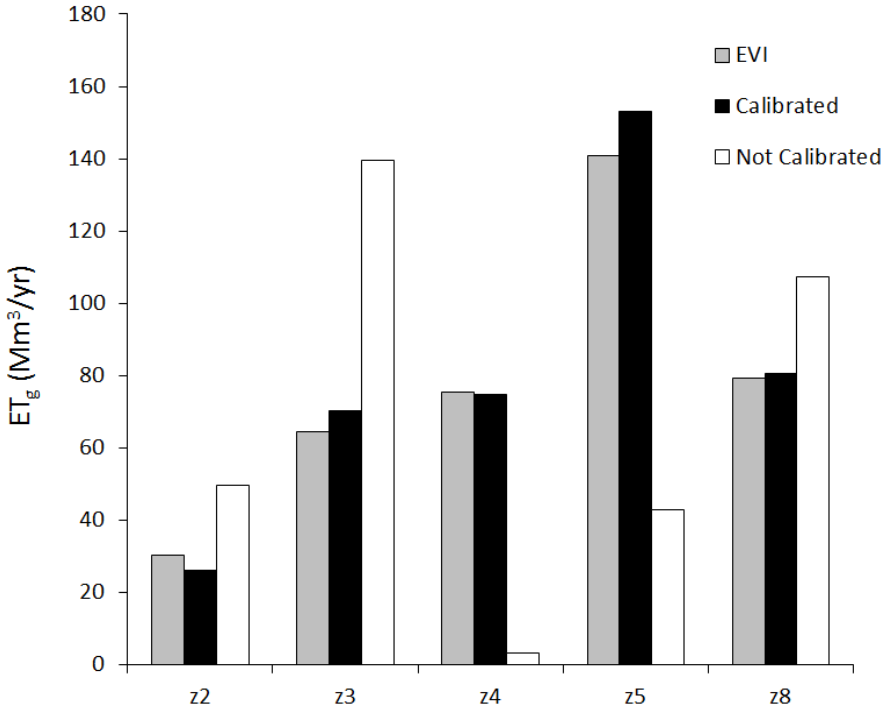

Figure 5. Total ET_g for each vegetation zone summed over years 1996-2006 (z2 = saltgrass, z3 = greasewood, z4 = wetland/open water, z5 = wetland riparian, z8 = river riparian).

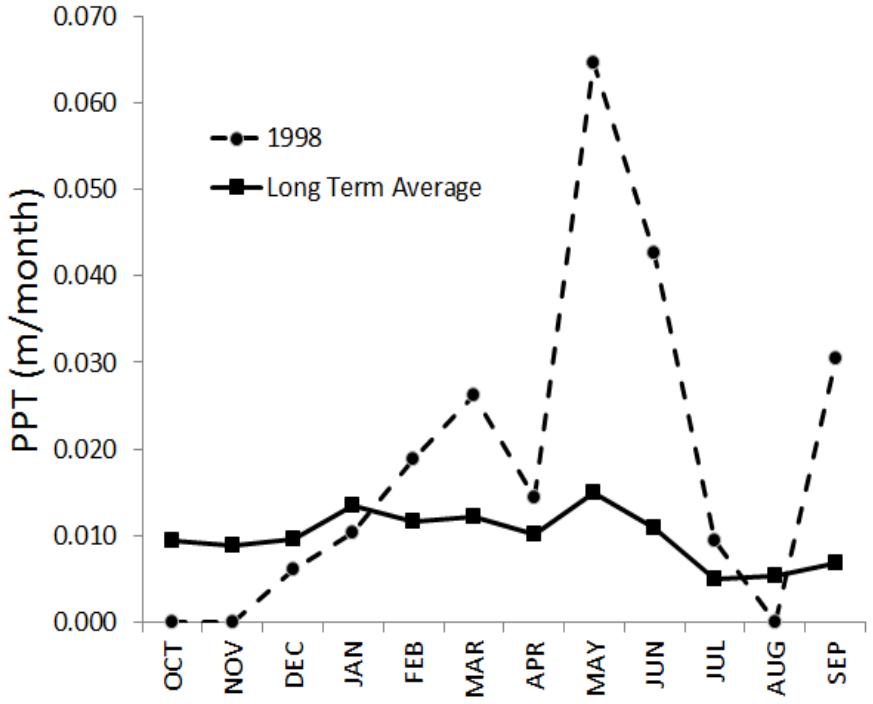

Figure 6. A comparison of 1998 and the long term average monthly PPT.

Model Uncertainty

GLUE generally does not require prior knowledge of the input parameter distribution. Instead, prior input distributions may, in theory, be assumed uniform and the methodology determines the posterior parameter distributions based on covariant relationships between input parameters and those combinations that are most influential in improving model performance. With respect to ET_g parameters, however, GLUE was unable to significantly modify prior input distributions and it became necessary to use expert judgment on designating these distributions. For instance, wide, uniform input distributions resulted in large uncertainty and were relatively insensitive to *N*. Normal input distributions with too narrow a standard deviation collapsed the uncertainty envelop such that the desired frequency of data captured by the CI could not be met. Consequently, if a parameter range was found too narrow in the GLUE analysis then the input prior distribution was re-designated as log-normal to enable an increase in the upper bound. Increasing *N* to 5 allowed a final adjustment of the CI by successfully collapsing the uncertainty envelop to capture 90% of the EVI derived ET_g data. Resulting posterior means (equation 11), standard deviations (equation 12), and 90% CI values for *HK*, α and *dx* parameters are given in Table 2. One thousand realizations were found adequate in establishing posterior μ values given convergence of mean values occurred to within ±1% after 800 realizations.

Table 2. Input parameter description and associated GLUE derived posterior means (μ), standard deviations (σ) and 90% confidence intervals. *HK* = hydraulic conductivity; α = PET_g scaling at land surface; *dx* = extinction depth.

Parameter	Description	Units	Prior Distribution	**Posterior**		**90% CI**	
				μ	**σ**	**Lower**	**Upper**
HK1	Upper River Sed.	m/d	Normal	9.89	9.52	4.70	14.99
HK2	Lower River Sed.	m/d	Normal	24.13	61.16	11.99	37.29
HK3	Young Alluv.	m/d	Log-Normal	1.45	1.03	0.17	3.66
HK4	Young Alluv. Fan	m/d	Log-Normal	1.19	0.87	0.16	2.97
α_2	Saltgrass	-	Log-Normal	0.33	0.02	0.13	0.61
α_3	Greasewood	-	Log-Normal	0.33	0.02	0.13	0.61
α_4	Wetland	-	Normal	1.10	0.01	0.98	1.23
α_5	Wetland Riparian	-	Normal	0.94	0.01	0.80	1.10
α_8	River Riparian	-	Normal	0.53	0.02	0.32	0.75
dx_2	Saltgrass	m	Normal	18.47	21.26	10.82	26.22
dx_3	Greasewood	m	Normal	17.69	19.19	10.59	25.42
dx_4	Wetland	m	Normal	18.16	23.41	10.43	26.37
dx_5	Wetland Riparian	m	Normal	12.77	10.93	7.47	18.48
dx_8	River Riparian	m	Normal	5.30	3.21	2.28	8.36

Posterior means and standard deviations from Table 2 were used in the FOSM analysis to calculate normalized sensitivity (S^*) and normalized relative uncertainty (U^*). FOSM results are plotted in Figure 7. Model uncertainty is driven by estimated variance (σ^2), with U^* in *dx*-terms impacting their respective vegetation group anywhere from 44% to 85%. Globally, dx_3 and dx_5 account for 36% of model uncertainty, while HK_1 and HK_2 account for the remaining 64%. Relative uncertainty of all α-terms amasses to only 0.02% relative uncertainty at the global level.

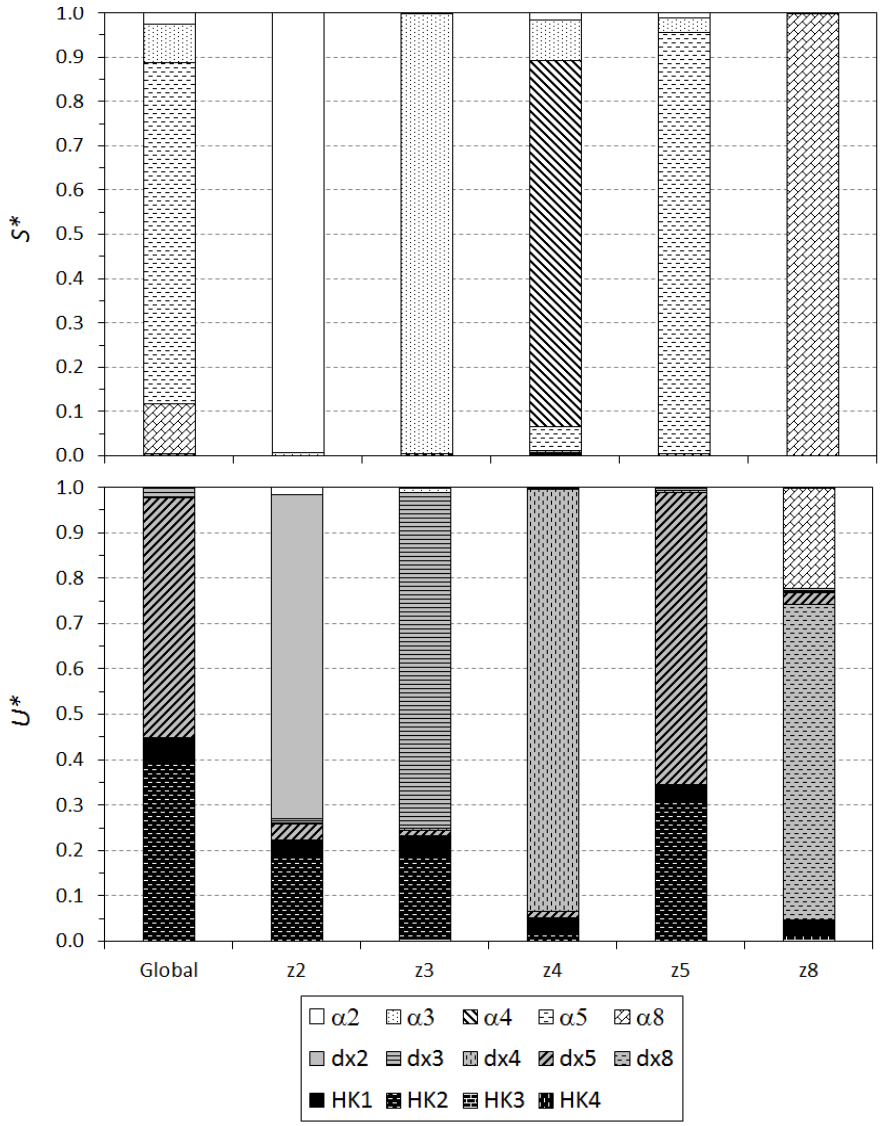

Figure 7. (a) normalized sensitivity and (b) normalized relative uncertainty expressed globally and for individual vegetation zones (z2 = saltgrass; z3 = greasewood; z4 = wetland open water; z5 = wetland riparian and z8 = river riparian). The α parameters are presented with a white background, *dx* parameters with a gray background and *HK* parameters with a black background.

Despite large uncertainty in *HK* on modeled ET_g volumes, model sensitivity is low, less than 0.23% globally, and *HK* uncertainty does not have any appreciable impact on estimated ET_g to *dtgw* relationships. This suggests that the ET_g and *HK* calibrations can be performed separately. Instead, model output sensitivity is dominated by α-terms. While each vegetation zone is highly sensitive to its respective α-term, globally α_5 is of greatest importance, accounting for 75% of the model output sensitivity. In contrast, the greasewood community (α_3) produces uncertainty nearly seven times less than the wetland riparian regions despite occupying 40% more area.

Figure 8 shows subsequent ψ to *dtgw* curves including the 90% CI. Plots are based on ψ, as opposed to ET_g. The transformation is done because ET_g and PET_g change with every stress period but ψ remains temporally constant for any given *dtgw*. Observed ψ to *dtgw* data obtained in wells located in regions containing greasewood or wetland riparian vegetation are superimposed in the graphs for zone 3 and zone 5, respectively.

Results show that it is not necessary to divide the saltgrass and greasewood communities into two distinct functional phreatophyte groups. Zones are based on dominant species, but at the 100 m cell size of the GWM, the saltgrass community is indistinguishable from the more aerially extensive greasewood community. The 90% CI for α indicates that the saltgrass-greaswood community uses a maximum of 13-61% PET_g as determined by ASCE grass reference, with a mean extinction depth between 11 and 26 m (Table 2, Fig 8a, 8b). Estimated extinction depths are too deep to represent saltgrass (Blaney et al., 1933; Cooper et al., 2006), but encompass literature reported values for greasewood with rooting depths reported from 11 m (Robertson, 1983; Mozingo, 1987) to 18 m (Robinson, 1958). Likewise, Nichols (1994) suggests extinction depths are larger than 14 m. Observed data show low ψ demand at shallow depths and very modest declines in ψ with increased *dtgw*. Observed data for wells 41 and 52 (refer to Fig. 1) scatter about the estimated mean and are contained within the 90% CI. Observed data for wells 4 and 5, however, occur near land surface, exhibit ψ <0.1, and fall below the lower bound of the CI. Model predictions of ψ at land surface (α) are driven by the need to include large volumes of ET_g derived from EVI images during water years 1998, 2005 and 2006 which, as already discussed, may not accurately represent vegetation vigor as a result of groundwater consumption. Removing these years from the analysis, or developing a methodology that accounts for both quantity and timing of annual precipitation on phreatophyte greenness and the resulting EVI index, would substantially reduce α for greasewood and allow a greater collapse in the 90% CI.

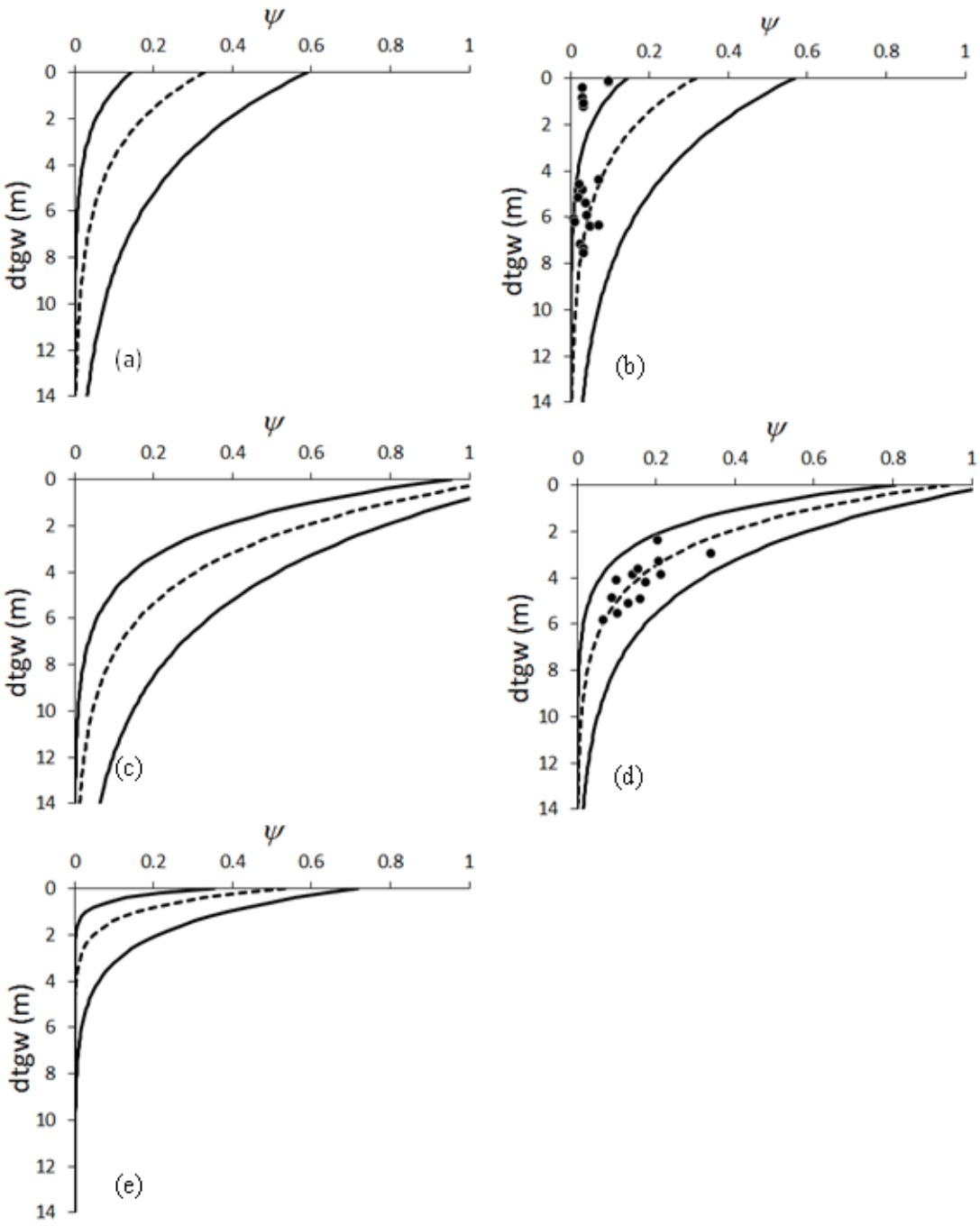

Figure 8. Resulting ψ to *dtgw* curves obtained in calibrating to EVI ET_g data, (a) saltgrass, zone 2, (b) greasewood, zone 3, (c) wetland/open water, zone 4, (d) wetland riparian, zone 5 and (e) river riparian, zone 8. Dashed and solid lines represent GLUE derived mean and 90% confidence intervals, respectively. Black circles are observed ψ to *dtgw* data.

Wetland riparian zones occupy the second largest area in the basin, behind greasewood, and exhibit the largest ET_g, with EVI estimates ranging from 9.5 to 15.5 Mm^3/yr (7,600 to 12,600 AFY). As expected, the ψ to *dtgw* curves representing wetland regions (Fig. 8c) and the riparian zone surrounding these wetlands (Fig. 8d) are very similar to each other, with ET_g nearly equal to the potential at land surface ($\alpha \sim 1.0$). Large α terms indicate large consumptive use by open water as well as surrounding riparian vegetation on the order of 0.006 m/d during the middle of summer. Micrometerological data collected in the Walker Basin (Allander et al., 2006) found maximum open water evaporation on the order of 0.100 m/d, willow *ET* reaching 0.009 m/d and salt cedar ranging from 0.001 m/d to 0.003 m/d. Additional comparisons show that GWM estimates of maximum riparian consumption fall near the upper *ET* ranges for salt cedar as estimated via eddy covariance (Dahm et al., 2002; Cleverly et al., 2002; 2006) and remote sensing (Nagler et al., 2008; 2009); as well as at the upper range for Cottonwood as estimated via sap flux (Schaeffer et al., 2000; Pataki et al., 2005). All comparative studies, however, represent actual *ET*, not groundwater derived ET_g, and GWM estimates appear large if considering the GLUE derived mean estimates, but satisfactory if considering the lower CI bound.

The 90% CI for extinction depths for wetlands and associated riparian vegetation are modeled from 7.5 m to 26 m below land surface. Modeled *dx* are deep compared to those reported by Baird and Maddock (2005) in which extinction depths are reported at 0.1 m for obligate vegetation, 1.5 m for shallow-rooted riparian vegetation, 5 m for deep-rooted vegetation and 6 m for transitional riparian vegetation. However, all basin specific data fall within the 90% CI (refer to Figure 8d) to independently verify the modeling approach for wetland riparian zones pertaining to Mason Valley and the spatial scale modeled.

The last vegetation group considered is the riparian zone along the river corridor where modeled water levels are often at or just below land surface. Results show relatively low consumption of groundwater at land surface with ψ approximately 50%, or 0.003 m/d during the summer months, and a shallow extinction depth (5 m) and narrow uncertainty envelope compared to other vegetation zones (Fig. 8e). Numerically, the low α and *dx* values and a narrow 90% CI reflect the need to substantially reduce ET_g through GWM calibration. No site-specific data exists for Mason Valley in this vegetation zone, but Baird and Maddock (2005) report maximum riparian ET_g on the order of 0.003 m/d, while modeled extinction depths are consistent with their published results for deep rooted riparian vegetation.

Large uncertainty occurs in estimated extinction depths for all functional groups. Numerically, large uncertainty in the extinction depth is most likely based on (1) the relative insensitivity of *dx* to modeled ET_g compared to α, (2) the 100 m resolution in the model allows for species, canopy cover and plant density variability, (3) land surface elevations in the model are defined by the mean land surface elevation for each 100 m grid cell to introduce variability in *dtgw* estimates, and (4) to the over-arching assumption that vegetation vigor (i.e. greenness) and ET_g are consistently proportional. With respect to the

latter, the modeling approach corrects ET_g for precipitation, but does not account for the timing of stored soil moisture in the EVI algorithm. It is likely that temporal variability in soil moisture is expressed in the model's uncertainty.

Additionally, the physiologic complexity of phreatophyte vegetation may add considerable variability in the extinction depth. Phreatophytes likely respond to both magnitude and rate of water table decline (Cooper et al., 2006). Rapid water table lowering of less than 1 m can cause significant reductions in ET_g in riparian phreatophytes such as Cottonwoods or by altering leaf area, branch density and whole plant density. In contrast, salt cedar may not be completely dependent on groundwater availability and may experience little change in vegetation vigor, or greenness, with a decline in water level (Busch et al., 1992). The response of phreatophyte species to a lowering of the water table may be based on a species ability to use soil water during a certain season, or their capacity to grow deeper roots in response to declining water levels, and this introduces uncertainty into model derived ψ to *dtgw* curves.

Conclusions

While ET_g often accounts for a majority of groundwater discharge from closed and semi closed basins in the arid and semi-arid regions in the southwest United States, most groundwater models are not calibrated to this loss term. *Ad hoc* modeling can potentially introduce large error in basin-scale water balances. For the Mason Valley example, the published GWM shows that with no calibration, saltgrass, greasewood, as well as river riparian vegetation, estimates of ET_g were overestimated, while wetland regions and their riparian zones were significantly under predicted. The methodology presented takes advantage of large scale vegetation mapping, remote sensing techniques and basin-scale groundwater models to help researchers and water managers better constrain phreatophyte and riparian ET_g at the basin scale. Atmospheric water demand and precipitation are tracked to acquire an estimate of potential ET_g for a reference crop and assumes an exponential decay function of ET_g with depth to the water table to limit model calibration to a two-parameter problem. While uncertainty in *HK* is large with respect to ET_g discharge volume, this uncertainty does not translate into uncertainty in ET_g to *dtgw* relationships. The significance of this finding is that *HK* and ET_g can be calibrated independently to greatly simplify the procedure.

GLUE incorporates the concept of equifinality such that different parameter sets can produce equally good, or acceptable, model behavior. However, in assessing ET_g, model performance is greatly impacted by choice of prior input distribution such that wide, uniform prior distributions are not capable of providing insight on model calibration or in quantifying input parameter uncertainty. Instead, manual calibration is required before GLUE to establish means for normal distributions, while the upper and lower bounds of these prior distributions may need some iterative adjustment to ensure adequate width of the CIs. While

N can fine tune the CI, its ability to control the CI width is limited. Instead, expert judgment in model calibration defines the prior input distribution that is critical to determining output CI.

The modeling approach proved robust by capturing basin-scale ET_g trends for different functional classes, and matching observed ψ to *dtgw* data. Future investigations need to develop a methodology to include the precipitation timing on vegetation vigor and impacts on EVI derived ET_g. It is believed this adjustment will better constrain the 90% CI for the greasewood ψ to *dtgw* curve. In addition, future work should also consider the transient response of phreatophytic ET_g to sustained water table declines caused by changing hydrologic regime. The complexity of vegetation response to sustained drawdown, and the associated impacts to ET_g are important for long-term water budget calculations but currently not incorporated into basin-wide studies of water resources.

Groeneveld (2008) is one of the few studies to correlate a normalized remotely sensed vegetation index to observed water levels to investigate ET_g as a function of *dtgw*. However, the resulting non-linear relationships, until now, have not been used directly in modeling studies at the basin scale. It is expected that the approach presented can update existing groundwater models in the southwestern United States as well as help develop more rigorous monitoring networks to aid in model development and calibration.

References Cited

Allander, K.K., Smith, J.L., Johnson, M.J., 2006. Evapotranspiration (ET) in the Lower Walker River Basin, west-central Nevada. Nevada Water Resources Association 2006 Annual Conference. Mesquite, NV. February 23.

Allander, K.K., Smith, J.L., Johnson, M.J., 2009. Evapotranspiration from the lower Walker River basin, west-central Nevada, water years 2005-07. U.S. Geological Survey Scientific Investigations Report 2009-5079, 62 pp.

Allen, R.G., 2011. RET-ET: Reference evapotranspiration calculation software for FAO and ASCE standardized equations. Version 3.1 for Windows. University of Idaho.

ASCE-EWRI, 2005. The ASCE Standardized Reference Evapotranspiration Equation. ASCE-EWRI Standardization of Reference Evapotranspiration Task Committee Report.

Baird, K.J., Maddock III, T., 2005. Simulating riparian evapotranspiration: a new methodology and application for groundwater models. J. Hydrol. 312, 176-190.

Banta, E.R., 2000. Modflow-2000, The U.S. Geological Survey modular ground-water model-documentation of packages for simulating evapotranspiration with a segmented function (ETS1) and drains with return flow (DRT1). U.S. Geological Survey Open-File Report 00-466, 131pp.

Beamer, J.P., Huntington, J.L., Morton, C.G., Pohll, G.M., in review. Estimation of annual groundwater evapotranspiration from phreatophyte vegetation in the Great Basin using Landsat EVI and flux tower measurements. J. Am. Water Resour. Assoc.

Beven, K.J., Binley, A.M., 1992. The future of distributed models: Model calibration and uncertainty prediction. Hydrol. Processes. 6, 279-298.

Blaney, H.F., Taylor, C.A., Young, A.A., Nickle, H.G., 1933. Water loses under natural conditions in wet areas in southern California, I, Consumptive use by native plants growing in moist areas of southern California, Bulletin. 44, pp. 19-139. Water Resources Division., Calif. Dep. of Public Works, Sacramento.

Blasone, R-S., Madsen, H., Rosbjerg, D., 2008. Uncertainty assessment of integrated distributed models using GLUE with Markov chain Monte Carlo sampling. J. Hydrol. 353, 18-32.

Busch, D.E., Ingraham, N.L., Smith, S.D., 1992. Water uptake in woody riparian phreatophytes of the southwestern United States: a stable isotope study. Ecological Applications. 2, 450–459.

Carroll, R.W.H., Pohll, G.M., McGraw, D., Garner, C., Knust, A., Boyle, D., Minor, T., Pohlmann, K., 2010. Mason Valley groundwater model: Linking surface water and groundwater in the Walker River Basin, Nevada. J. Am. Water Resour. Assoc. 46(3), 554-573.

Cleverly, J.R., Dahm, C.N., Thibault, J.R., McDonnell, D.E., Allred Coonrod, J.E., 2006. Riparian ecohydrology: regulation of water flux from the ground to atmosphere in the Middle Rio Grande, New Mexico. Hydrol. Processes. 20, 3207-3225.

Cleverly, J.R., Dahm, C.N., Thibault, J.R., Gilroy, D.J., Allred Coonrod, J.E., 2002. Seasonal estimates of actual evapotranspiration from *Tamarix ramosissima* stands using three-dimensional eddy covariance. J. Arid Environ. 52, 181-197.

Cooper, D.C., Sanderson, J.S., Stannard, D.I, Groeneveld, D.P., 2006. Effects of long-term water table drawdown on evapotranspiration and vegetation in an arid region phreatophyte community. J. Hydrol. 325, 21-345.

Dahm, C.N., Cleverly, J.R., Allred Coonrod, J.E., Thibault, J.R., McDonnell, D.E., Gilroy, D.J., 2002. Evapotranspiration at the land/water interface in a semi-arid drainage basin. Freshwater Biol. 47, 831-843.

Devitt, D.A., Donovan, D.J., Katzer, T., Johnson, M., 2002. A reevaluation of the ground water budget for Las Vegas Valley, Nevada, with emphasis on ground water discharge. J. Am. Water Resour. Assoc. 38, 1735-1751.

Franks, S.W., Beven, K.J. and Gash, J.H. 1999. Multi-objective conditioning of a simple SVAT model. Hyd. Earth Sys. Sci. 3(4): 477-489.

Groeneveld, D.P., 2008. Remotely-sensed groundwater evapotranspiration from alkali scrub affected by declining water table. J. Hydrol. 358, 294-303.

Groeneveld, D.P., Baugh, W.M., 2007. Correcting satellite data to detect vegetation signal for eco-hydrologic analyses. J. Hydrol. 344, 135-145.

Groeneveld, D.P., Baugh, W.M., Sanderson, J.S., Cooper, D.J., 2007. Annual groundwater evapotranspiration mapped from single satellite scenes. J. Hydrol. 344, 146-156.

Harbaugh, A.W., Banta, E.R., Hill, M.C., McDonald, M.G., 2000. MODFLOW-2000, the U.S. Geological Survey modular ground-water model – User guide to modularization concepts and the Ground-Water Flow Process. U.S. Geological Survey Open-File Report 00-92, 121 pp.

Harr, R.D., Price, K.R., 1972. Evapotranspiration from a greasewood-cheatgrass community. Water Resour. Res. 8(5), 1199-1203.

Hess, R.H., Johnson, G.L., 1997. County Digital Geologic Maps of Nevada (GIS format). Nevada Bureau of Mines and Geology, Open File Report 97-1, CD Rom.

Huete, A., Didan, K., Miura, T., Rodriguez, E.P., Gao, X., Ferreira, L.G., 2002. Overview of the radiometric and biophysical performance of the MODIS vegetation indices. Remote Sens. Environ. 83, 195-21.

Huntington, J.L., Szilagyi, J., Tyler, S.W., Pohll, G.M., 2011. Evaluating the complementary relationship for estimating evapotranspiration from arid shrublands. Water Resour. Res. 47, W05533.

Huntington, J.L., Allen, R.G., 2010. Evapotranspiration and net irrigation water requirements for Nevada. State of Nevada Department of Conservation and Natural Resources, Division of Water Resources. 288 pp. http://water.nv.gov

Huxel, J.C.J., Harris, E.E., 1969. Water resources and development in Mason Valley, Lyon and Mineral Counties 1948-65. Water Resources Bulletin 38, U.S. Geological Survey, Department of Conservation and Natural Resources.

Laczniak, R.J., Smith, J.L., Elliott, P.E., DeMeo, G.A., Chatigny, M.A., Roemer, G.J., 2001. Ground-water discharge determined from estimates of evapotranspiration, Death Valley Regional Flow System, Nevada and California. U.S. Geological Survey Water-Resources Investigations Report 01-4195, 57pp.

Laczniak, R.J., DeMeo, G.A., Reiner, S.R., Smith, J.L., Nylund, W.E., 1999. Estimates of ground-water discharge as determined from measurements of evapotranspiration, Ash Meadows Area, Nye County, Nevada. U.S. Geological Survey Water-Resources Investigations Report 99-4079, 77pp.

Malmberg, G.T., 1967. Hydrology of the valley-fill and carbonate-rock reservoirs, Pahrump Valley, Nevada– California. U.S. Geological Survey Water-Supply Paper 1832, 47 pp.

Malmberg, G.T., Eakin, T.E., 1962. Ground-water appraisal of Sarcobatus Flat and Oasis Valley, Nye and Esmeralda Counties, Nevada. Nevada Department of Conservation and Natural Resources, Ground-Water Resources Reconnaissance Series Report 10, 39 pp.

Masek, J.G., Vermote, E.F., Saleous, N.E., Wolfe, R., Hall, F.G., Huemmrich, K.F., Gao, F., Kutler, J., Lim, T., 2006. A Landsat surface reflectance dataset for North America, 1990-2000. IEEE Geosci. Remote Sens. Lett. 3, 68-72.

Maurer, D.K., Berger, D.L., Tumbusch, M.L., Johnson, M.J., 2006. Rates of evapotranspiration, recharge from precipitation beneath selected areas of native

vegetation, and streamflow gain and loss in Carson Valley, Douglas County, Nevada, and Alpine County, California. U.S. Geological Survey Scientific Investigations Report 2005-5288, 70 pp.

Minor, T., Bassett, S., Kratt, C., Trammell, E.J., 2006. Great Basin land and water Walker Lake Basin Study: GIS study of trends in irrigated lands in the Walker Lake Basin. Desert Research Institute, Division of Earth and Ecosystem Sciences.

Moreo, M.T., Laczniak, R.J., Stannard, D.I., 2007. Evapotranspiration rate measurements of vegetation typical of groundwater discharge areas in the Basin and Range carbonate-rock aquifer system, White Pine County, Nevada, and adjacent areas in Nevada and Utah, September 2005–August 2006. U.S. Geological Survey Scientific Investigations Report 2007-5078, 36 pp.

Mozingo, H.N., 1987. Shrubs of the Great Basin. University of Nevada Press, Reno, Nevada. 342 pp,

Nagler, P.L., Morino, K., Didan, K., Erker, J., Osterberg, J., Hultine, K.R., Glenn, E.P., 2009. Wide-area estimates of saltcedar (*Tamarix* spp.) evapotranspiration on the Lower Colorado River measured by heat balance and remote sensing methods. Ecohydrology. 2, 18-33.

Nagler, P.L., Glenn, E.P., Didan, K., Osterberg, J., Cunningham, J., 2008. Wide-area estimates of stand structure and water use of *Tamarix* on the Lower Colorado River: Implications for restoration and water management. Restoration Ecology. 16, 136–145.

Nagler, P.L., Scott, R.L., Westenburg, C., Cleverly, J.R., Glenn, E.P., Huete, A.R., 2005. Evapotranspiration on Western U.S. rivers estimated using the enhanced vegetation index from MODIS and data from eddy covariance and Bowen Ratio flux towers. Remote Sens. Environ. 97(3), 337-351.

Nichols, W.D., 2000. Regional groundwater evapotranspiration and groundwater budgets, Great Basin, Nevada. U.S. Geological Survey Professional Paper 1628, 82 pp.

Nichols, W.D., 1994. Groundwater discharge by phreatophyte shrubs in the Great Basin as related to depth to groundwater. Water Resour. Res. 30(12), 3265-3274.

Pataki, D.E., Bush, S.E., Gardener, P., Solomon, D.K., Ehleringer, J.R., 2005. Ecohydrology in a Colorado River riparian forest: implications for the decline of *Populus fremontii*. Ecological Applications. 15, 1009–1018.

Robertson, J.H., 1983. Greasewood (*Sarcobatus vermiculatis* (Hook.) Torr.). Phytologia. 54(5), 309-324.

Robinson, T.W., 1958. Phreatophytes. U.S. Geological Survey Water Supply Paper 1423, 84 pp.

Rush, F.E., 1968. Water-resources appraisal of Clayton Valley- Stonewall Flat area, Nevada and California. Nevada Department of Conservation and Natural Resources, Water Resources-Reconnaissance Series Report 45, 54 pp.

Schaeffer, S.M., Williams, D.G., Goodrich, D.C., 2000. Transpiration of cottonwood/willow forest estimated from sap flux. Agricultural and Forest Meteorology. 105, 241–256.

Shah, N., Mahmood, N., Ross, M., 2007. Extinction depth and evapotranspiration from ground water under selected land covers. Ground Water. 45, 329-338.

Smith, J.L., Laczniak, R.J., Moreo, M.T., Welborn, T.L., 2007. Mapping evapotranspiration units in the Basin and Range Carbonate-Rock Aquifer System, White Pine County, Nevada, and adjacent areas in Nevada and Utah. U.S. Geological Survey Scientific Investigations Report 2007-5087, 31 pp.

Walker, G.E., Eakin, T.E., 1963. Geology and ground water of Amargosa Desert, Nevada-California. Nevada Department of Conservation and Natural Resources, Ground Water Resources-Reconnaissance Report 14, 45 pp.

Western Regional Climate Center (WRCC), 2007. Yerington long term average precipitation record 1/1/1914 to 12/31/2007, station 269229. http://www.wrcc.dri.edu/cgi-bin/cliMAIN.pl?nvyeri.